The Astrophysical Journal, 962:145 (7pp), 2024 February 20 https://doi.org/10.3847/1538-4357/ad18d7

The Search for Failed Supernovae with the Large Binocular Telescope: The Mid-infrared Counterpart to N6946-BH1

Christopher S. Kochanek[1,2], Jack M. M. Neustadt[1], and Krzysztof Z. Stanek[1,2]
[1] Department of Astronomy, The Ohio State University, 140 W. 18th Ave., Columbus, OH 43210, USA; kochanek.1@osu.edu
[2] Center for Cosmology and AstroParticle Physics, The Ohio State University, 191 W. Woodruff Ave., Columbus, OH 43210, USA
Received 2023 October 11; revised 2023 December 21; accepted 2023 December 25; published 2024 February 15

Abstract

We present JWST MIRI 5.6, 10, and 21 μm observations of the candidate failed supernova N6946-BH1 along with Hubble Space Telescope (HST) WFPC/IR 1.1 and 1.6 μm data and ongoing optical monitoring data with the Large Binocular Telescope. There is a very red, dusty source at the location of the candidate, which has only $\sim$10%–15% of the luminosity of the progenitor star. The source is very faint in the HST near-IR observations ($\sim 10^3 L_\odot$) and is not optically variable to a limit of $\sim 10^3 L_\odot$ at the R band. The dust is likely silicate and probably has to be dominated by very large grains, as predicted for dust formed in a failed supernova. The required visual optical depths are modest, so it should begin to significantly brighten in the near-IR over the next few years.

Unified Astronomy Thesaurus concepts: Black hole physics (159); Massive stars (732)

Supporting material: machine-readable table

1. Introduction

The formation rate of stellar mass black holes (BHs) is a critical unknown for the physics of massive stars, supernovae (SNe), nucleosynthesis, the origin of X-ray (and other) binaries, and gravitational wave sources. In modern theories of massive star death, most stellar mass BHs form in failed SNe without a high luminosity explosion. Stars generally either explode to form a neutron star, or they do not, and form a BH (e.g., O'Connor & Ott 2011; Ugliano et al. 2012; Ertl et al. 2016; Sukhbold et al. 2016). These models suggest that 10%–30% of core collapses lead to a failed SN. This is supported by the lack of higher mass SN progenitors (Kochanek et al. 2008; Smartt et al. 2009, but see Davies & Beasor 2020 and Kochanek 2020).

For red supergiants (RSGs), a failed SN should have a weak transient in which most of the hydrogen envelope is ejected to leave a BH with roughly the mass of the helium core (e.g., Lovegrove & Woosley 2013; Lovegrove et al. 2017; Fernández et al. 2018; Ivanov & Fernández 2021; Antoni & Quataert 2023), with significant dust formation in the ejected envelope (Kochanek 2014a). The ejection of the envelope in a failed SN of an RSG to leave a BH with the mass of the helium core provides the first natural explanation of the 5–10$M_\odot$ BHs found in the Galaxy (Kochanek 2014b, 2015).

Measuring the rate of BH formation and failed SNe is challenging because the most unambiguous signatures would be neutrino or gravitational wave observations of the collapse. Such observations will only be possible in our Milky Way Galaxy and its satellites for the foreseeable future. But if the Galactic SN rate is roughly one per century, there is a failed SN only once every 300–1000 yr (see, e.g., Adams et al. 2013).

In Kochanek et al. (2008), we proposed the one presently feasible approach to finding failed SNe. With an 8 m class telescope, we can search for RSGs that vanish in a failed SN independent of the nature of any intermediate transient. We have been carrying out this program for 15 yr (Gerke et al. 2015; Adams et al. 2017a; Neustadt et al. 2021), finding one very good candidate (Gerke et al. 2015) and one weaker candidate (Neustadt et al. 2021). If we just count the strong candidate, this implies a failed SN rate of $f_{\rm SN} = 0.16^{+0.23}_{-0.12}$ at 90% confidence, which is consistent with theoretical expectations (Neustadt et al. 2021). It is reassuring that the number of candidates is small, because this means that there are few or no other sources that mimic the vanishing of an RSG in a failed SN.

The best candidate, named N6946-BH1 for its host galaxy and status as the first candidate, had a weak transient in 2009 and then rapidly faded to become optically invisible to levels $<$1% of the pretransient luminosity. Prior to the transient, the progenitor had a nearly constant optical luminosity that could be traced back to the late 1990s. When Basinger et al. (2021; and previously Adams et al. 2017b) last did a detailed study, they found no optical counterpart to limits of $\lesssim 10^3 L_\odot$ or less, a low-luminosity fading near-IR counterpart ($\sim 2000 L_\odot$), and no mid-IR counterpart ($\lesssim 10^4 L_\odot$) compared to an estimated progenitor luminosity of $\simeq 10^{5.6} L_\odot$.

Basinger et al. (2021) were left with two issues. First, the Spitzer mid-IR constraints were weaker than desirable, subject to problems from confusion due to their low angular resolution, and could only constrain the presence of relatively warm dust emission since they provided measurements only at 3.6 and 4.5 μm. While obscuration of a star by an ongoing dusty wind and some models of obscuration by dust formed in the 2009 transient could be ruled out, the limits could be evaded by simply making the dust more distant and colder at the price of pushing the ejecta mass and kinetic energies upwards into a physically challenging regime if the present-day luminosity is the same as the progenitor luminosity. Second, if a BH was formed, it should have an extended period of accretion, and very little mass fallback is required to produce significant emission since the Eddington limit for a 10$M_\odot$ BH is $10^{5.5} L_\odot$ (coincidentally matching the

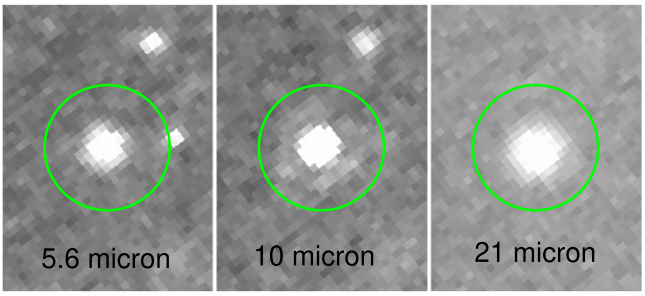

Figure 1. The JWST MIRI F560W (left), F1000W (middle), and F2100W (right) images of N6946-BH1. The continued brightness of BH1 toward longer wavelengths compared to the nearby stars demonstrates that the emission is due to dust. North is up and the circles are $1\farcs0$ in radius.

progenitor luminosity) and only requires an accretion rate of $\dot{M} = 2 \times 10^{-7} M_\odot\,\mathrm{yr}^{-1}$ for an efficiency of 10%. However, the accretion rates are not well determined, particularly in the scenario of a failed SN (e.g., Perna et al. 2014; Quataert et al. 2019; Antoni & Quataert 2022, 2023).

Here, we report on new JWST MIRI mid-IR observations, Hubble Space Telescope (HST) WFPC3/IR near-IR observations, and continuing Large Binocular Telescope (LBT) optical monitoring observations of NGC 6946 BH1. We describe the data and their reduction in Section 2. Beasor et al. (2023) reported results of their independent JWST observations of the same source taken one month earlier. We focus on modeling our data and compare to their results where appropriate. We model the resulting spectral energy distribution (SED) and discuss the implications in Section 3, and summarize the results in Section 4. We adopt the same distance, 7.7 Mpc (Anand et al. 2018), and extinction, $E(B-V) = 0.303$ (Schlafly & Finkbeiner 2011), used by Basinger et al. (2021). The distance is consistent with the 7.8 Mpc distance found using the tip of the red giant branch by Murphy et al. (2018).

2. Data

We obtained HST WFPC3/IR F110W (J) and F160W (H) images on 2023 January 29 with three dithered images in each band and total integration times of 1350 s for both bands. We obtained JWST MIRI F560W (5.6 μm), F1000W (10 μm), and F2100W (21 μm) images on 2023 September 26 with effective exposure times of 87, 87, and 526 s. We used the BRIGHT-SKY region with four dither positions. For F560W and F1000W, we used one integration with 25 groups for each image, while for F2100W we used three integrations each with 50 groups. We also have an ongoing optical monitoring program with the LBT. The JWST images are shown in Figure 1, the sequence of HST near-IR images we have obtained are shown in Figure 2, and the LBT R-band light curve is shown in Figure 3 and in Table 1.

The mid-IR source is well isolated, so we used the STScI pipeline photometry for the fluxes. These show small variations ($\sim$10%) between apertures, which are unimportant given that we are interested in the logarithmic value of the luminosity. We did do our own aperture and point-spread function photometry as a check of the pipeline values, finding good agreement. We obtained fluxes of 17.6 ± 1.8, 40.6 ± 0.3, and 87 ± 1 μJy for the F560W, F1000W, and F2100W bands, respectively. The F560W flux is $\sim$50% of

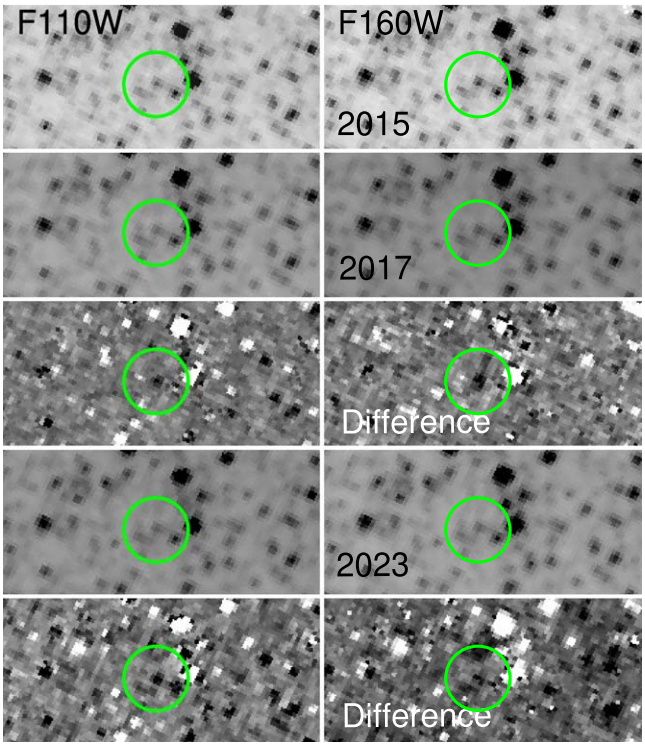

Figure 2. The HST F110W (left) and F160W (right) observations from 2015 (top), 2017 (middle), and 2023 (bottom) along with the difference images between the 2017/2023 epochs and the 2015 epoch. Black in the difference images means the source has faded relative to 2015. North is up and the circles are $1\farcs0$ in radius centered on NGC 1646-BH1.

the Beasor et al. (2023) value, while the other two fluxes agree well. We used difference imaging (Alard & Lupton 1998; Alard 2000) to analyze the new HST data, as this provides excellent sensitivity to changes in brightness even in the very crowded near-IR environment of BH1. We estimate current F110W and F160W magnitudes of 24.34 and 22.61 (dominated by systematic errors) where the source faded slightly at F110W and brightened slightly at F160W compared to 2017. The LBT data are processed using standard methods, as described in Gerke et al. (2015), Adams et al. (2017a), and Neustadt et al. (2021), and analyzed using difference imaging following Alard & Lupton (1998) and Alard (2000). We find that the optical flux cannot have changed by more than $\sim 10^3 L_\odot$ at the R band since the transient faded in 2010–2011.

We will fit our MIRI results and use our new HST near-IR results and the earlier HST optical results from Adams et al. (2017b) as upper limits. Beasor et al. (2023) find that the HST resolution near-IR source seems to be three similar luminosity sources at JWST resolution. This is consistent with the difference between our HST/F160W luminosity estimates and their NIRCAM/F185W estimates, but our HST/F110W luminosities match their NIRCAM/F115W estimates. Since they also argue that their NIRCAM/F250M fluxes must be off by a factor of $\sim$2.6, we decided to just focus on our data. We are mainly concerned with the bulk energetics, and the exact values of these near-IR fluxes are not important to the basic result, although they are crucial to the future evolution of the source, as we discuss in Section 4.

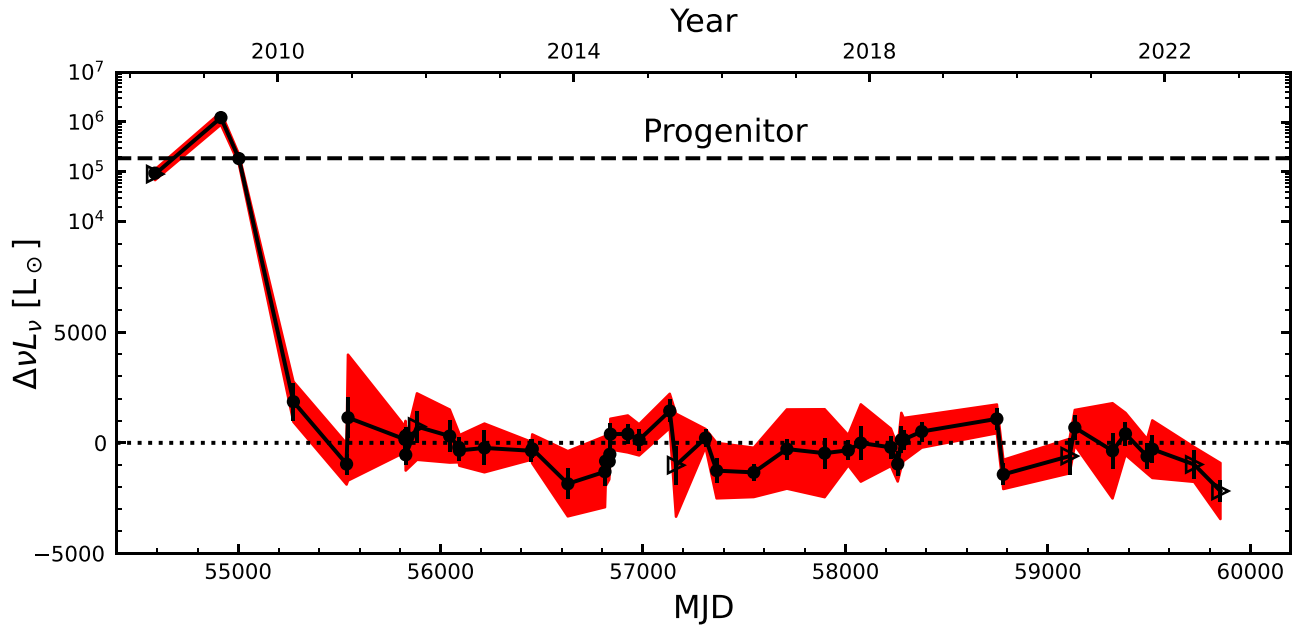

Figure 3. The LBT *R*-band light curve of N6946-BH1. After the optical transient ends in 2010, there have been no optical changes at the level of a few $10^3 L_\odot$ or roughly 1% of the progenitor luminosity. Triangles are epochs with poor visibility or lower transparency (clouds/cirrus).

Table 1
R-band Light Curve of N6946-BH1 Using LBT

MJD	L ($L_\odot$)	σ_L ($L_\odot$)	Flag
54589.45	93830	24150	1
54590.42	89810	21520	0
54915.51	1224950	338400	1
55004.32	184330	40000	1
55273.51	1860	910	1
55536.08	–960	920	1
…	…	…	…
59516.21	–290	1300	1
59722.45	–980	780	0
59852.22	–2180	1260	0

Note. Flag corresponds to data quality (1 = good, 0 = bad data due to poor observing conditions). L and σ_L are rounded to the nearest 10 $L_\odot$.
(This table is available in its entirety in machine-readable form.)

3. Results

Following our approach in Adams et al. (2017b) and Basinger et al. (2021), we model the SED with DUSTY (Ivezic & Elitzur 1997; Ivezic et al. 1999; Elitzur & Ivezić 2001), a spherically symmetric dust radiation transfer program. We model the underlying source using a Castelli & Kurucz (2003) model stellar atmosphere with a luminosity of L_* and a temperature of T_*. The dust is distributed as a $\rho \propto r^{-2}$ shell from $R_{\rm in}$ to $R_{\rm out} = 2R_{\rm in}$. In our previous studies, we have found that the results are insensitive to the choice of $R_{\rm out}$ because the optical depth is dominated by the inner regions. We use Draine & Lee (1984) graphitic and silicate dusts and start with a Mathis et al. (1977) $a^{-3.5}$ grain size distribution spanning $0.005 < a < 0.25\,\mu$m. The dust parameters are the visual optical depth τ_V through the shell, and the dust temperature T_d at the inner edge. The dust temperature combined with L_* then determines $R_{\rm in}$, from which we can estimate the ejecta velocity $v_e \simeq R_{\rm in}/\Delta t$, where we adopt $\Delta t = 14$ yr. Following Adams et al. (2017b), DUSTY is embedded in a Markov Chain Monte Carlo "wrapper," which is used to optimize the fits to the SED and estimate uncertainties. For the most part, parameter uncertainties are not an important part of our story.

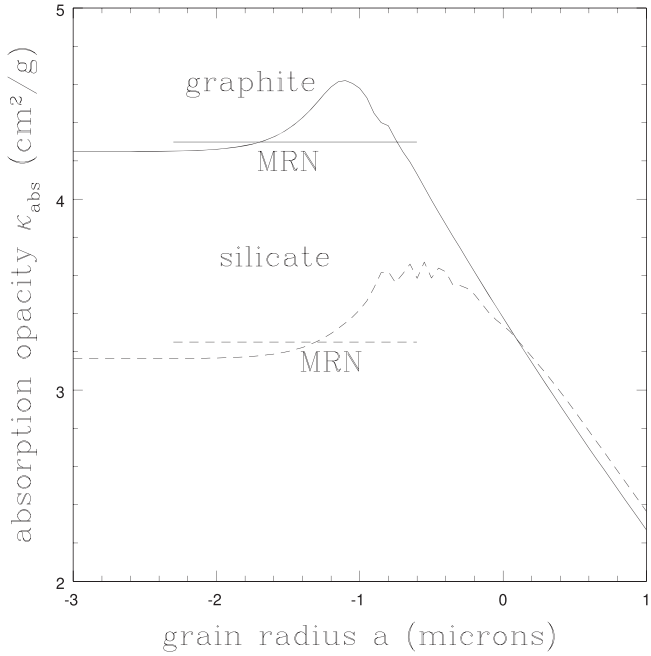

Figure 4. The *V*-band (0.55 μm) absorption opacities, $\kappa_{\rm abs}$, for Draine & Lee (1984) graphitic (solid) and silicate (dashed) dusts. The horizontal lines show the mean for the default DUSTY (Mathis et al. 1977) $a^{-3.5}$ size distribution with $0.005 < a < 0.25\,\mu$m (the size range spanned by the line).

Figure 4 shows the *V*-band (0.55 μm) absorption opacities, $\kappa_{\rm abs}$, per unit dust mass for the Draine & Lee (1984) graphitic and silicate dusts along with their averages for the Mathis et al. (1977) size distribution. For consistency with DUSTY, we assume a bulk dust density of 3 g cm^{-3} and a gas-to-dust ratio of $f_{\rm gd} = 200$. The opacity per unit gas mass is then the opacity

per unit dust mass shown in Figure 4 divided by $f_{\rm gd}$. The Mathis et al. (1977) averaged absorption opacities per unit gas mass are then $\kappa_V \simeq 98\,{\rm cm^2\,g^{-1}}$ and $10\,{\rm cm^2\,g^{-1}}$ for the graphitic and silicate dusts, respectively. The ejecta gas mass is then

$$M_{\rm e} = \frac{4\pi R_{\rm in} R_{\rm out}\tau_V}{\kappa_V} = 0.63\tau_V \frac{R_{\rm out}}{R_{\rm in}}\left(\frac{R_{\rm in}}{10^{17}\,{\rm cm}}\right)^2\left(\frac{100\,{\rm cm^2\,g^{-1}}}{\kappa_V}\right)M_\odot \quad (1)$$

and the ejecta kinetic energy is

$$K_{\rm e} = \frac{2\pi R_{\rm in}^3 R_{\rm out}\tau_V}{\Delta t^2\kappa_V} = 0.032\tau_V \frac{R_{\rm out}}{R_{\rm in}}\left(\frac{R_{\rm in}}{10^{17}\,{\rm cm}}\right)^4\left(\frac{100\,{\rm cm^2\,g^{-1}}}{\kappa_V}\right){\rm FOE}, \quad (2)$$

where FOE $= 10^{51}$ erg. For the estimates of $M_{\rm e}$ and $K_{\rm e}$, we just use $R_{\rm out} = R_{\rm in}$, since we have no real constraints on $R_{\rm out}$. This means that the estimates are lower bounds on the mass and the kinetic energy.

We fit the SEDs assuming stellar temperatures of $T_* = 4000$, 7000, 10,000, 15,000, and 20,000 K. With no information on the structure of the optical SED, there is no way to determine T_*. We fit the SED treating the optical (F606W and F814W) and near-IR (F110W and F160W) HST luminosities as upper limits and vary T_d, τ_V, and L_* to fit the MIRI luminosities. We include no additional host extinction. The primary effect of adding a host extinction is that it drives up the estimate of the progenitor luminosity while having a negligible effect on the mid-IR luminosity observed today. This would exacerbate the differences between the present-day and progenitor luminosities.

The key comparison for these models is between the luminosity implied by the current SED and that of the progenitor. Here, we compare to the progenitor properties found using MARCS (Gustafsson et al. 2008) stellar atmospheres fit to the archival HST F606W and F814W data from 2007 along with the nearly concurrent Spitzer 3.6 and 4.5 μm images (see Adams et al. 2017b). We use the MARCS models here because the preferred temperatures lie close to the lowest temperatures in the Castelli & Kurucz (2003) models. Models with no dust fit reasonably well with $T_* \simeq 3500$ K and $L_* = 10^{5.63} L_\odot$. The photometric constraints and the progenitor SED model are shown in Figures 5 and 6. Models with a little hot dust ($T_d \simeq 1300$ K, $\tau_V \simeq 0.2$) fit a little better, but the stellar parameters change little ($T_* \simeq 3500$ K, $L_* - 10^{5.62} L_\odot$). The higher luminosity here and in Basinger et al. (2021) is driven by using a larger distance (7.7 versus 6.0 Mpc) than Adams et al. (2017b). Beasor et al. (2023) find that the near-IR source breaks up into three sources at the resolution of JWST, but this has no impact on estimates of the luminosity of the progenitor as it was over an order of magnitude more luminous than these contaminating sources in the near-IR.

These initial models are really focused on the possibility of a surviving star surrounded by "normal" dust. The primary difference from Adams et al. (2017b) and Basinger et al. (2021) is that the mid-IR emission now constrains the actual present-day luminosity. Figures 5 and 6 show the SEDs and their models for graphitic and silicate dust, respectively, for all five source temperatures T_*. The models are able to fit the mid-IR fluxes while staying below the optical/near-IR limits for both dust types and all stellar temperatures. As expected, the input spectrum largely only matters in the near-IR, where the limits force any contribution to the overall luminosity to be modest. The mid-IR SEDs vary only a little bit with T_* and this is mostly due to the freedom created by the luminosity uncertainties. The mid-IR SEDs differ between the dust types

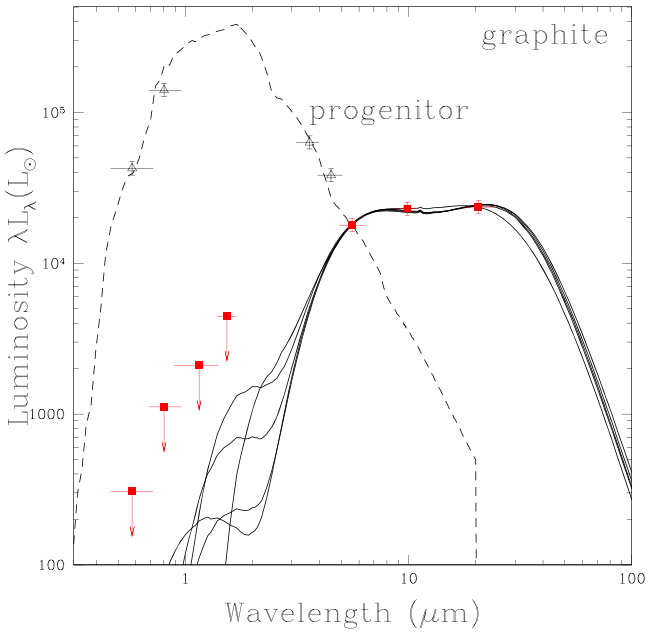

Figure 5. The present-day SED of NGC 6946 (filled red points and limits) modeled with graphitic dust (solid curves) for stellar temperatures of $T_* = 4000$, $T_* = 7000$, $T_* = 10{,}000$, $T_* = 15{,}000$, and $T_* = 20{,}000$ K. The progenitor SED and its model are shown by the open triangles and dashed curve. The horizontal bars on the points are the filter widths.

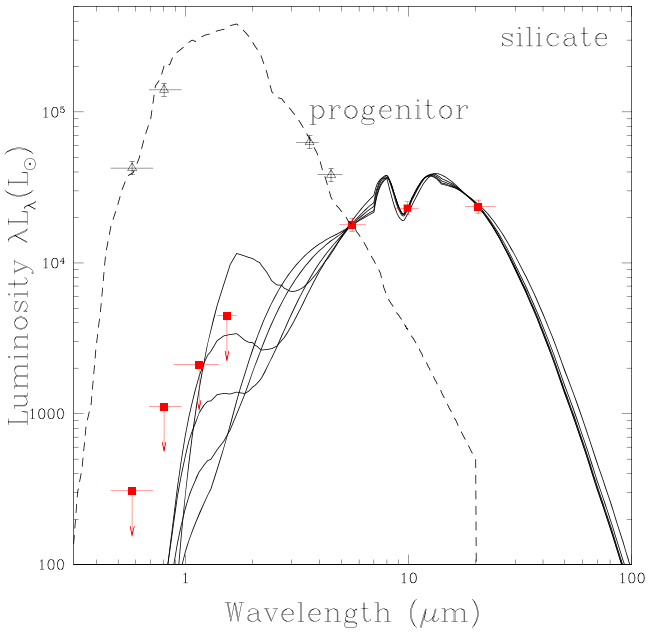

Figure 6. The present-day SED of NGC 6946 (filled red points and limits) modeled with silicate dust (solid curves) for stellar temperatures of $T_* = 4000$, $T_* = 7000$, $T_* = 10{,}000$, $T_* = 15{,}000$, and $T_* = 20{,}000$ K. The progenitor SED and its model are shown by the open triangles and dashed curve. The horizontal bars on the points are the filter widths.

because the silicate dusts have a feature near 10 μm while the graphitic dusts do not. The graphitic dusts have a flat SED at the peak, while the silicate dusts produce a double-peaked SED with the 10 μm data lying in the valley between the peaks. The silicate models predict that a peak should be seen at 7 μm in the F770W band, and this is exactly what Beasor et al. (2023) observed. This indicates that the dusts are likely the silicate dusts expected for massive RSGs.

The model luminosities are almost exactly the same, with a range of $10^{4.70} L_\odot$ to $10^{4.80} L_\odot$. This means that the present-day luminosity is only 10%–15% of the progenitor luminosity, and the survival of the progenitor is essentially ruled out. The visual optical depths are functions of both the dust type and T_*, with lower optical depths for graphitic dust and higher temperatures. But, at least for these models, they are not extreme, with $\tau_V = 6.9$ to 38 for the graphitic dusts and $\tau V = 19$ to 33 for the silicate dusts. The dust temperatures would be better constrained with measurements at 2–3 μm, but range from a minimum of $T_d \simeq 420$ to a maximum of 1000 K. The dust radius depends on the stellar temperature because the Planck absorption factors $Q(T_*)$ are larger for hotter stars, forcing the dust to be more distant for higher stellar temperatures. For the graphitic dusts, the radii are in the range $R_{\rm in} = 10^{15.8}$ to $10^{16.3}$ cm and for the silicate dusts they are all roughly $10^{15.5}$ cm. This implies relatively slow expansion velocities of 150–500 km s^{-1} for the graphitic models and $\sim$80 km s^{-1} for the silicate models. Because the optical depths are modest and the low luminosity allows $R_{\rm in}$ to be relatively small, the necessary ejecta masses are small, $M_e \sim 0.1$ to $0.2 M_\odot$, which, combined with the low velocities, means the kinetic energies are also small compared to SN energies, $\sim 10^{-5}$ to 5×10^{-4} FOE.

The low masses may seem Sproblematic for a failed SN interpretation even if the velocities are of the right order of magnitude. Given the near-IR detections, the problem cannot be solved by simply increasing the optical depth, nor is preventing dust formation a likely solution (see Section 4). The solution has to lie in the opacity, in particular from using the Mathis et al. (1977) grain size distribution. In the Kochanek (2014a) failed SN dust formation models, there are very few grains in the Mathis et al. (1977) size range—98% of the dust mass is in grains bigger than 10 μm. Since the large grains have optical Planck factors $Q \simeq 1$, their absorption cross sections are simply $\propto a^2$ while their masses are $\propto a^3$, so all of the dust mass is in big grains while the absorption is still dominated by smaller grains. If we simply extend the maximum grain size, the silicate absorption opacities per unit gas mass drop from $\kappa_{\rm abs} \simeq 10$ to 5.4, 1.9m, and 0.6 cm^2 g^{-1} for $a_{\rm max} = 10$, 100, and 1000 μm, as seen in Figure 4. Figure 2 in Kochanek (2014a) shows that only the outermost, lowest density layers of the ejecta produce grains smaller than 1 μm. With an additional small change in the size distribution from Mathis et al. (1977) in favor of larger grains, it appears likely that the visual opacities can be driven down far enough to allow ejecta masses of many $M_\odot$. As seen in Figure 7, extending the grain size distributions to very large values of $a_{\rm max}$ has little effect on the SED model.

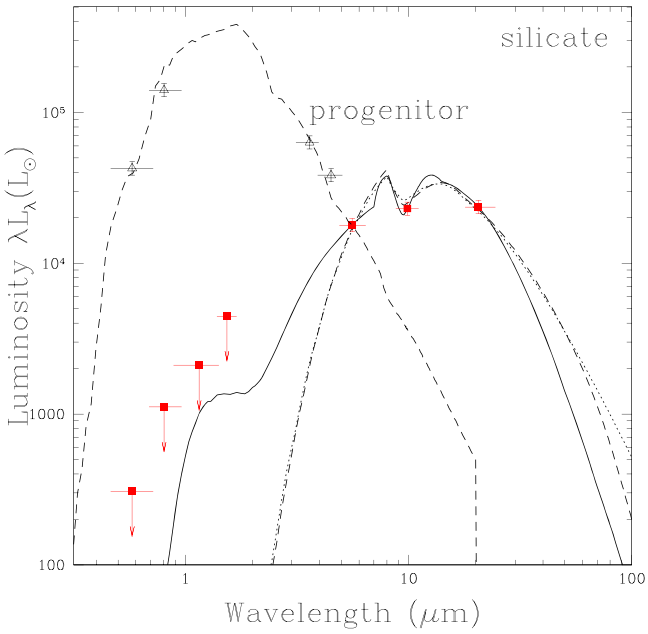

Figure 7. The present-day SED of NGC 6946 (filled red points and limits) modeled with silicate dust (solid curves) for a stellar temperature of $T_* = 10{,}000$ K and the grain distribution stopping at $a_{\rm max} = 0.25$ μm (solid), 10 μm (dashed), and 1000 μm (dotted). The progenitor SED and its model are shown by the open triangles and dashed curve. The horizontal bars on the points are the filter widths.

4. Discussion

While we make no use of the Beasor et al. (2023) data, we note that essentially all of our silicate dust models predict enhanced emission at 7.7 μm compared to 5.6 and 10 μm, which is what they found. The usual logic for dust formation is that the type of dust is determined by the abundance of carbon relative to oxygen. The two elements will preferentially bind to make CO, and then graphitic dusts are made if there is leftover carbon and silicate dusts are made if there is leftover oxygen. In the MIST stellar models (Paxton et al. 2011, 2013, 2015; Choi et al. 2016; Dotter 2016), the envelopes of RSGs are all oxygen-rich. RSG winds are also observed to be dominated by oxide dusts like the silicates (e.g., Verhoelst et al. 2009) and the same would be expected for dust formed in the ejected envelope since the winds simply have the composition of the envelope. They need not be simply silicate dusts, but exploring additional types is beyond our present scope.

As discussed in Adams et al. (2017b), the optical luminosity of the progenitor was fairly steady over the decade prior to the transient in 2009. Adams et al. (2017b) fit SEDs including Spitzer mid-IR constraints and found no significant change in the bolometric luminosity between 2005 July and 2008 July, although there may have been some modest changes in a dusty wind. So there is no good evidence for the premerger luminosity variations seen in V1309 Sco (Tylenda et al. 2011). The brightness changes in V1309 Sco were also quite modest, about 1 mag at the I band, with most of that occurring in the last $\sim$3 yr. In our case, the R-band optical luminosity was steady for the last decade, particularly compared to the order of magnitude difference between the luminosity of the progenitor and the luminosity today. The energetically less important B and V bands varied more, fading in the last few years combined with a rise in the mid-IR emission, consistent with a change in the wind optical depth but at a nearly constant bolometric luminosity. It is, of course, presently popular to invoke mass loss changes in RSGs shortly before core collapse (e.g., Bostroem et al. 2023 for SN 2023ixf recently).

Kashi & Soker (2017) argue that obscuring the system with a dusty disk viewed edge on would allow most of the luminosity to escape in the polar directions and thus significantly reduce the total observed flux, thereby breaking the link between the observed luminosity and the luminosity of the underlying source. Beasor et al. (2023) also invoke this concept as part of their argument for making this system a stellar merger. However, Adams et al. (2017b) had already demonstrated for the limiting case of a slab geometry that this idea does not work in practice. More recently, Kochanek (2023) carried out a detailed investigation of dust radiation transfer in disky geometries and found that, even for extremely high disk optical depths (up to $\tau_V = 10^3$, orders of magnitude larger than needed here), the luminosity inferred by an observer in the disk plane was at most a factor of 2 different from the true luminosity. It is also difficult to suppress the optical flux by the extreme factors needed here (see Figures 3, 5, and 6), because even a small amount of polar dust will scatter a detectable amount of optical light to the observer.

V1309 Sco largely demonstrates this point because the progenitor was an eclipsing binary, and hence our viewing angle is close to the plane of the orbit (Tylenda et al. 2011). While the optical emission dropped to be fainter than the progenitor in roughly two years, the total luminosity remained $\sim$60 times greater than the pre-event luminosity ($\sim 9 L_\odot$) four years after peak (Tylenda & Kamiński 2016). By 2017, an epoch roughly comparable to our present observations, its *I*-, *J*-, and K_s-band luminosities were 3.2, 2.5, and $0.4 L_\odot$ (Ferreira et al. 2019), so its total luminosity in just these three bands approaches the total luminosity of the progenitor. V838 Mon also shows a disk-like structure (Chesneau et al. 2014; Kamiński et al. 2021; Mobeen et al. 2021) but never became significantly fainter than the progenitor and it presently has a similar *B*-band flux to the progenitor and is brighter at the *V* band (compare Munari et al. 2005 and Liimets et al. 2023). This is complicated by the presence of a triple companion, but it is argued that the star producing the transient was the more luminous. Based on Munari et al. (2005), the progenitor luminosity would be $\sim 10^4 L_\odot$, and the present-day luminosity including the dust emission (e.g., Woodward et al. 2021) appears to be comparable or higher.

Beasor et al. (2023) express concerns that the X-ray and ultraviolet radiation produced by accretion would destroy the dust. This is an issue when grains are first forming because high energy photons can stochastically heat small grains above the evaporation temperature and suppress dust formation (Kochanek 2011). For an existing grain, the energy of an ionizing photon is shared over many atoms/bonds because it is deposited by a fast electron Coulomb scattering through the grain. The electron loses its energy over a distance $\simeq 0.01 E_{\rm keV}^{1.5}$ μm for a photon of energy $E_{\rm keV}$ keV (Draine & Salpeter 1979), which is nearly $10^6 E_{\rm keV}^{1.5}$ atomic spacings—the energy deposited per atom/bond is actually quite small. Grain shattering by electrically charging the grains due to interactions with X-rays may be feasible, but requires the very high fluences of γ-ray bursts (see Waxman & Draine 2000; Fruchter et al. 2001). Moreover, even if the accretion luminosity commenced immediately, the sheer amount of ejected mass protects most of the ejecta during the dust formation phase. For example, if we have material expanding at 200 km s^{-1}, one solar mass of hydrogen has a column density of $2 \times 10^{26} t_{\rm year}^{-2}$ cm^{-2}, which is Compton thick for over a decade (see the discussion on X-ray absorption in Basinger et al. 2021). Similarly, the inner layers of gas would absorb all the ionizing ultraviolet flux for an extended period of time. In short, the inner gas protects the outer gas while it forms dust and, once the dust is formed, it basically does not care about the energy of the photons.

Thus, we argue that the simplest explanation remains interpreting N6946-BH1 as a failed SN currently powered by accretion luminosity. But it is a hypothesis that should certainly undergo additional tests. It would be nice to find additional pre-event observations hiding in various archives, but this seems unlikely at this point. This really only leaves continued monitoring of the source, and these observations and those of Beasor et al. (2023) make it clear that this needs to be done with JWST. While we have no constraints from our observations on the NIRCAM filters, we do find a significantly different ($\sim$50%) flux in our MIRI F560W fluxes (we agree on the 10 and 21 μm fluxes). Variability seems to be a natural consequence of accretion, so a JWST monitoring campaign should be informative. Densely filling in the SED with all the available NIRCAM/MIRI filters should clarify the nature of the dust, and a mid-IR spectrum could likely be obtained in a reasonable integration time. But, in the end, time may be the only fundamental test—either we fade to black, or we do not. The optical depths we infer are not tremendously high, and mass conservation requires the dust optical depth to drop at least as fast as $\tau \propto t^{-2}$—so even on a one-year timescale, a visual optical depth of $\tau_V = 20$ should drop to $\tau_V \simeq 17.5$ and the corresponding *K*-band optical depth of $\tau_K \simeq 2$ would drop to $\tau_K = 1.7$—any underlying source should become significantly brighter in the near-IR over the next few years.

Acknowledgments

J.M.M.N. thanks A. Ash and J. Roberts for help with the MIST models. J.M.M.N. and C.S.K. are supported by NSF grants AST-2307385 and AST-1908570. Support for programs JWST GO-2896 and HST GO-17144 was provided by NASA through a grant from the Space Telescope Science Institute, which is operated by the Association of Universities for Research in Astronomy, Inc., under NASA contract NAS 5-03127. This work is based (in part) on observations made with the NASA/ESA/CSA James Webb Space Telescope. The data were obtained from the Mikulski Archive for Space Telescopes at the Space Telescope Science Institute, which is operated by the Association of Universities for Research in Astronomy, Inc., under NASA contract NAS 5-03127 for JWST. These observations are associated with program GO-2896. This research is based on observations made with the NASA/ESA Hubble Space Telescope obtained from the Space Telescope Science Institute, which is operated by the Association of Universities for Research in Astronomy, Inc., under NASA contract NAS 526555. These observations are associated with program(s) GO-17144. The LBT is an international collaboration among institutions in the United States, Italy, and Germany. LBT Corporation partners are: The University of Arizona on behalf of the Arizona university system; Istituto Nazionale di Astrofisica, Italy; LBT Beteiligungsgesellschaft, Germany, representing the Max-Planck Society, the Astrophysical Institute Potsdam, and Heidelberg University; The Ohio State University, and The Research Corporation, on behalf of The University of Notre Dame, University of Minnesota, and University of Virginia.

Data Availability

The HST and JWST data will be publicly available after the standard proprietary period. The HST and JWST data from programs HST GO-14266, HST GO-15311, HST GO-17144, and JWST GO-2896 are linked by doi:10.17909/g88z-0t38.

Facilities: HST, JWST, LBT.

ORCID iDs

Christopher S. Kochanek https://orcid.org/0000-0001-6017-2961
Jack M. M. Neustadt https://orcid.org/0000-0001-7351-2531

References

Adams, S. M., Kochanek, C. S., Beacom, J. F., Vagins, M. R., & Stanek, K. Z. 2013, ApJ, 778, 164
Adams, S. M., Kochanek, C. S., Gerke, J. R., & Stanek, K. Z. 2017a, MNRAS, 469, 1445
Adams, S. M., Kochanek, C. S., Gerke, J. R., Stanek, K. Z., & Dai, X. 2017b, MNRAS, 468, 4968
Alard, C. 2000, A&AS, 144, 363
Alard, C., & Lupton, R. H. 1998, ApJ, 503, 325
Anand, G. S., Rizzi, L., & Tully, R. B. 2018, AJ, 156, 105
Antoni, A., & Quataert, E. 2022, MNRAS, 511, 176
Antoni, A., & Quataert, E. 2023, MNRAS, 525, 1229
Basinger, C. M., Kochanek, C. S., Adams, S. M., Dai, X., & Stanek, K. Z. 2021, MNRAS, 508, 1156
Beasor, E. R., Hosseinzadeh, G., Smith, N., et al. 2023, arXiv:2309.16121
Bostroem, K. A., Pearson, J., Shrestha, M., et al. 2023, ApJL, 956, L5
Castelli, F., & Kurucz, R. L. 2003, in IAU Symp. 210, Modelling of Stellar Atmospheres, ed. N. Piskunov (Cambridge: Cambridge Univ. Press), A20
Chesneau, O., Millour, F., De Marco, O., et al. 2014, A&A, 569, L3
Choi, J., Dotter, A., Conroy, C., et al. 2016, ApJ, 823, 102
Davies, B., & Beasor, E. R. 2020, MNRAS, 493, 468
Dotter, A. 2016, ApJS, 222, 8
Draine, B. T., & Lee, H. M. 1984, ApJ, 285, 89
Draine, B. T., & Salpeter, E. E. 1979, ApJ, 231, 77
Elitzur, M., & Ivezić, Ž. 2001, MNRAS, 327, 403
Ertl, T., Janka, H. T., Woosley, S. E., Sukhbold, T., & Ugliano, M. 2016, ApJ, 818, 124
Fernández, R., Quataert, E., Kashiyama, K., & Coughlin, E. R. 2018, MNRAS, 476, 2366
Ferreira, T., Saito, R. K., Minniti, D., et al. 2019, MNRAS, 486, 1220
Fruchter, A., Krolik, J. H., & Rhoads, J. E. 2001, ApJ, 563, 597
Gerke, J. R., Kochanek, C. S., & Stanek, K. Z. 2015, MNRAS, 450, 3289
Gustafsson, B., Edvardsson, B., Eriksson, K., et al. 2008, A&A, 486, 951
Ivanov, M., & Fernández, R. 2021, ApJ, 911, 6
Ivezic, Z., & Elitzur, M. 1997, MNRAS, 287, 799
Ivezic, Z., Nenkova, M., & Elitzur, M., 1999, DUSTY: Radiation Transport in a Dusty Environment, Astrophysics Source Code Library, ascl:9911.001
Kamiński, T., Tylenda, R., Kiljan, A., et al. 2021, A&A, 655, A32
Kashi, A., & Soker, N. 2017, MNRAS, 467, 3299
Kochanek, C. S. 2011, ApJ, 743, 73
Kochanek, C. S. 2014a, MNRAS, 444, 2043
Kochanek, C. S. 2014b, ApJ, 785, 28
Kochanek, C. S. 2015, MNRAS, 446, 1213
Kochanek, C. S. 2020, MNRAS, 493, 4945
Kochanek, C. S. 2023, arXiv:2305.11936
Kochanek, C. S., Beacom, J. F., Kistler, M. D., et al. 2008, ApJ, 684, 1336
Liimets, T., Kolka, I., Kraus, M., et al. 2023, A&A, 670, A13
Lovegrove, E., & Woosley, S. E. 2013, ApJ, 769, 109
Lovegrove, E., Woosley, S. E., & Zhang, W. 2017, ApJ, 845, 103
Mathis, J. S., Rumpl, W., & Nordsieck, K. H. 1977, ApJ, 217, 425
Mobeen, M. Z., Kamiński, T., Matter, A., Wittkowski, M., & Paladini, C. 2021, A&A, 655, A100
Munari, U., Henden, A., Vallenari, A., et al. 2005, A&A, 434, 1107
Murphy, J. W., Khan, R., Williams, B., et al. 2018, ApJ, 860, 117
Neustadt, J. M. M., Kochanek, C. S., Stanek, K. Z., et al. 2021, MNRAS, 508, 516
O'Connor, E., & Ott, C. D. 2011, ApJ, 730, 70
Paxton, B., Bildsten, L., Dotter, A., et al. 2011, ApJS, 192, 3
Paxton, B., Cantiello, M., Arras, P., et al. 2013, ApJS, 208, 4
Paxton, B., Marchant, P., Schwab, J., et al. 2015, ApJS, 220, 15
Perna, R., Duffell, P., Cantiello, M., & MacFadyen, A. I. 2014, ApJ, 781, 119
Quataert, E., Lecoanet, D., & Coughlin, E. R. 2019, MNRAS, 485, L83
Schlafly, E. F., & Finkbeiner, D. P. 2011, ApJ, 737, 103
Smartt, S. J., Eldridge, J. J., Crockett, R. M., & Maund, J. R. 2009, MNRAS, 395, 1409
Sukhbold, T., Ertl, T., Woosley, S. E., Brown, J. M., & Janka, H. T. 2016, ApJ, 821, 38
Tylenda, R., Hajduk, M., Kamiński, T., et al. 2011, A&A, 528, A114
Tylenda, R., & Kamiński, T. 2016, A&A, 592, A134
Ugliano, M., Janka, H.-T., Marek, A., & Arcones, A. 2012, ApJ, 757, 69
Verhoelst, T., van der Zypen, N., Hony, S., et al. 2009, A&A, 498, 127
Waxman, E., & Draine, B. T. 2000, ApJ, 537, 796
Woodward, C. E., Evans, A., Banerjee, D. P. K., et al. 2021, AJ, 162, 183